Int. J. Heat Mass Transfer. Vol. 24, pp. 35–46

0017-9310/81/0101-0035 $02.00/0

THE TWO- AND THREE-DIMENSIONAL DISPERSAL OF A PASSIVE SCALAR IN A TURBULENT BOUNDARY LAYER

S. EL TAHRY and A. D. GOSMAN
Department of Mechanical Engineering, Imperial College, London, U.K.
and
B. E. LAUNDER
Department of Mechanical Engineering, University of California, Davis, CA 95616, U.S.A.

(*Received* 27 *March* 1979 *and in revised form* 6 *June* 1979)

Abstract – A numerical calculation scheme is described for predicting the transport of a passive scalar contaminant through a turbulent boundary layer. The scheme incorporates an algebraic stress closure for the turbulent stresses and heat fluxes based on the model of references [9–11]. A feature of the numerical treatment is the use of different finite-difference grids for the velocity and scalar fields each of which may expand independently in the down-wind direction so as just to cover the regions where significant gradients exist in the relevant dependent variables. Computations are reported for the diffusion of line and point sources with both ground and elevated releases. Calculations are generally in encouraging agreement with the measured behaviour.

NOMENCLATURE

a_{ij}^m, convection/diffusion coefficients in finite-difference concentration equation ($m \equiv P, N, S, E, W, U$);

a_j^n, convection/diffusion coefficients in finite-difference equations for temperature and hydrodynamic variables ($n = P, N, S, U$, respectively);

C, c, mean and fluctuating pollutant concentrations, respectively;

$C_1, C_2, C_3, C_1', C_2', C_s'$, constants appearing in the modelled Reynolds-stress equations;

$C_{1c}, C_{2c}, C_{1c}', C_{2c}'$, constants appearing in the modelled turbulent scalar flux equation;

$C_{\varepsilon 1}, C_{\varepsilon 2}, C_{\varepsilon s}$, constants appearing in the modelled dissipation rate equation;

D_{ij}, D_{ic}, D_k, diffusion fluxes $-\overline{u_i u_j}$ and $\overline{u_i c}$ and turbulence kinetic energy, respectively;

k, turbulence kinetic energy;

l, turbulence length scale;

$\mathbf{n}_i$, unit vector normal to the ground;

P, P_{ij}, P_c, P_{ic}, production of k, $\overline{u_i u_j}$ $\overline{c^2}$ and $\overline{u_i c}$, respectively;

R, residual of finite-difference solution;

R_k, ratio of generation to dissipation of turbulence energy;

S_j^u, source term in finite-difference equation;

U, u, mean and fluctuating velocities, respectively;

X_2, lateral distance from the plane of symmetry to the edge of concentration grid;

X_3, height of the upper boundary of the hydrodynamic grid;

X_3^l, X_3^u, heights of the lower and upper edges of the concentration grid, respectively;

x_i, coordinates in the Cartesian frame of reference.

Greek symbols

β, height of maximum concentration location;

β_2, height in the plane of symmetry where $C = 0.75\, C_{\max}$;

β_3, lateral displacement of location where $C = 0.75\, C_{\max}$;

Γ, diffusion coefficient;

δ, boundary layer thickness;

δ_{ij}, Kronecker delta;

ε, ε_{ij}, ε_{ic}, ε_c, dissipation rate of k, $\overline{u_i u_j}$, $\overline{u_i c}$ and $\overline{c^2}$, respectively;

η, normalised vertical coordinate of concentration grid;

η_h, normalised vertical coordinate of hydrodynamic grid;

κ, von Karman constant;

λ_2, λ_3, lateral and vertical locations where $C = 0.5\, C_{\max}$, respectively;

μ, molecular viscosity;

ν, kinematic viscosity;

ξ, normalised lateral coordinate of concentration grid;

ρ, density;

τ_w, wall shear stress;

ϕ_{ij}, approximation of the pressure-scrambling term in $\overline{u_i u_j}$ equation;

ϕ_{ijm} ($m = 1, 2$), components of ϕ_{ij} (excluding wall effects);

ϕ_{ijw}, components of ϕ_{ij} due to wall effects;

ϕ_{ic}, approximation of pressure-scalar gradient in $\overline{u_i c}$ equation;
ϕ_{icm} $(m = 1, 2)$, components of ϕ_{ic} (excluding wall effects);
ϕ_{icw}, components of ϕ_{ic} due to wall effects.

Superscripts and subscripts

$\hat{}$, denotes ensemble average;
i, denotes coordinate direction ($i = 1, 2, 3$, refer to streamwise, vertical and lateral directions, respectively);
i, j, k, pertaining to nodal location in finite-difference grid at $x_{1,i}\, x_{2,j}\, x_{3,k}$;
max, indicates maximum value.

1. INTRODUCTION

GENERAL concern at the release of pollutants into the atmosphere together with the advent of nuclear energy and its hazards have emphasized the need to be able to calculate downwind concentrations of pollutant emitted from sources into the atmosphere. Due to the complexity of the flow in the earth's boundary layer, attempts at estimating the dispersal characteristics have in the past relied on drastically simplified mathematical and physical models supported by experimental data of one kind or another. The earliest and still the most widely used approach to dispersal prediction is the 'Gaussian Plume Model', details of which can be found in Pasquill [1] or Slade [2]. With this scheme, the atmospheric surface layer is regarded as statistically steady and homogeneous while the distribution of concentration is supposed to have Gaussian characteristics. Rates of plume spread are supplied from consolidated experimental data recorded over a wide range of atmospheric stability conditions [1].

Although the Gaussian plume method is easy to use and inexpensive, the assumption of homogeneity severely restricts its applicability. For example, the method is not capable of simulating the effects of different levels of surface roughness or of variations of surface conditions with downstream distance. Further, the fact that the spread of the plume is dependent on the height of release (Davar [3]), makes it necessary to assemble a large body of empirical rate of spread data. In practice the only comprehensive data available are for ground level releases.

Other approaches have been based on analytical solutions of the time-averaged transport equation for the pollutant concentration C:

$$\rho U_1 \frac{\partial C}{\partial x_1} = \frac{\partial}{\partial x_2}\left(\Gamma_2 \frac{\partial C}{\partial x_2}\right) + \frac{\partial}{\partial x_3}\left(\Gamma_3 \frac{\partial C}{\partial x_3}\right). \quad (1)$$

Here x_1, x_2 and x_3 are the Cartesian coordinates in the wind direction and the lateral and vertical directions respectively, U_1 is the wind velocity, while Γ_2 and Γ_3 denote the effective turbulent diffusivities in the x_2 and x_3 directions. Several investigators (e.g. Smith [4] and Yih [5]) have obtained analytical solutions to equation (1) assuming power-law variations of the mean velocity and the turbulent diffusivities with height. In practice the need to restrict distributions to forms that allow analytical solutions is a severe drawback to this type of analysis. By contrast, numerical methods of solution allow more realistic physical assumptions and also open the possibility of simultaneously predicting the behaviour of both the pollutant plume and the boundary layer for arbitrary boundary conditions. An initial step in this direction has been taken by Ragland and Dennis [6] who obtained numerical solutions to equation (1), with a fully implicit, finite difference scheme, for the case of an elevated point source in a two dimensional boundary layer.

More recently, Catton and Wassel [7] employed a modified version of Patankar and Spalding's [8] boundary layer procedure to predict dispersal from a line source. Their analysis solved simultaneously the transport equations for streamwise momentum, for pollutant and (for thermally stratified flows) potential temperature. To calculate the turbulent diffusivities, a mixing length hypothesis was used which incorporated a rudimentary modification for buoyant effects.

The present contribution adopts the same general approach as Wassel and Catton but has chosen a more capacious framework both for modelling the turbulent transport mechanisms and for handling the numerical simulation. The turbulence model employed is a simplification of the second-moment closure of [9–11] involving the solution of transport equations for the turbulence energy k and its rate of dissipation ε. An important feature of the model is that anisotropies in the effective diffusivities emerge naturally from the system of equations as do likewise influences of buoyancy. There have been several numerical studies of different aspects of the atmospheric boundary layer with this type of closure (e.g. [12–14]) though only Lewellyn and Teske [15] appear to have employed such a model for studying pollutant dispersal. The latter contribution provides several interesting predictions of pollutant transport but provides little firm comparison with experiment.

Although the present procedure is ultimately intended for application to atmospheric dispersal, the present contribution limits attention to the simulation of various wind-tunnel dispersion studies under essentially neutral conditions. These data, we believe, provide a more reliable and well-defined testing ground than the atmospheric measurements.* The specific situations considered are steady, point or line sources of pollutant emitted into a two-dimensional, turbulent boundary layer flowing over a plane surface whose roughness may vary in the downstream direction but not laterally. The momentum of the plume fluid is assumed to be small enough not to disturb significantly the boundary layer.

*It is, however, recognized that several important features of atmospheric dispersion are not reproduced in the wind tunnel.

2. THE MATHEMATICAL AND PHYSICAL MODEL

2.1. *The conservation equations*

The dispersal of a passive scalar contaminant in a statistically stationary, two-dimensional turbulent flow without body forces is governed by the following set of transport equations:

Continuity:

$$\frac{\partial \rho U_1}{\partial x_1} + \frac{\partial \rho U_3}{\partial x_3} = 0 \tag{2}$$

Streamwise Momentum:

$$\frac{\partial}{\partial x_1}\rho U_1 U_1 + \frac{\partial}{\partial x_3}\rho U_3 U_1 = -\frac{\partial}{\partial x_3}\left(\overline{\rho u_1 u_3} - \mu\frac{\partial U_1}{\partial x_3}\right) - \frac{\partial P}{\partial x_1} \tag{3}$$

Scalar Concentration:

$$\frac{\partial}{\partial x_1}\rho U_1 C + \frac{\partial}{\partial x_3}\rho U_3 C = -\frac{\partial}{\partial x_2}\left(\overline{\rho u_2 c} - \Gamma\frac{\partial C}{\partial x_2}\right) - \frac{\partial}{\partial x_3}\left(\overline{\rho u_3 c} - \Gamma\frac{\partial C}{\partial x_3}\right). \tag{4}$$

In the above, u_i denotes a fluctuating velocity in direction x_i about the mean value U_i and c is the corresponding fluctuation about the mean concentration. The correlations $\overline{u_1 u_3}$, $\overline{u_2 c}$ and $\overline{u_3 c}$ represent the momentum and concentration fluxes due to the turbulent motion. They are at present unknowns to the system of equations; approximations are provided in the next section.

Due to the large differences in the dimensions of the plume and the boundary layer it turns out to be advantageous to use two distinct, intermeshed grids for the solution. Equations (2) and (3) are solved on a coarse grid spanning the whole boundary layer while equation (4) is solved on a separate fine grid. The grids expand independently so as just to encompass the region where significant gradients exist in the quantities being calculated. To facilitate the introduction of the expanding grids, the equations are recast in terms of two new sets of independent variables. For the concentration field we replace the Cartesian coordinates by x, ξ, η where

$$x = x_1; \quad \xi = x_2/X_2; \quad \eta = (x_3 - X_3^l)/(X_3^U - X_3^l),$$

where X_2, X_3, X_3^U and X_3^l are reference distances which will be prescribed more precisely later. Correspondingly, the velocity field is described in terms of coordinates x and η_h where

$$\eta_h = x_3/X_3.$$

On transforming to the new coordinate system, equations (2–4) may be written:

$$\frac{\partial U_1}{\partial x} - \frac{1}{X_3}\eta_h\frac{\partial \rho U_3}{\partial \eta}\frac{dX_3}{dx} + \frac{1}{X_3}\frac{\partial \rho U_3}{\partial \eta_h} = 0, \tag{5}$$

$$\frac{\partial U_1 U_1}{\partial x} - \frac{1}{X_3}\eta_h\frac{\partial U_1 U_1}{\partial \eta_h}\frac{dX_3}{dx} + \frac{1}{X_3}\frac{\partial U_1 U_3}{\partial \eta_h} = -\frac{1}{X_3}\frac{\partial}{\partial \eta_h}\left(\overline{u_3 u_1} + \frac{\nu}{X_3}\frac{\partial U_1}{\partial \eta_h}\right) - \frac{1}{\rho}\frac{dP}{dx}, \tag{6}$$

$$\frac{\partial U_1 C}{\partial x} - \frac{1}{X_3^U - X_3^l}\frac{\partial U_1 C}{\partial \eta}\left(\eta\frac{dX_3^U}{dx} - \frac{dX_3^l}{dx}(1-\eta)\right) - \frac{1}{X_2}\xi\frac{\partial U_1 C}{\partial \xi}\frac{dX_2}{dx} + \frac{1}{X_3^U - X_3^l}\frac{\partial U_3 C}{\partial \eta} = -\frac{1}{X_3^U - X_3^l}\frac{\partial}{\partial \eta}\left(\overline{u_3 c} - \frac{\nu_c}{X_3^U - X_3^l}\frac{\partial C}{\partial \xi}\right) - \frac{1}{X_2}\frac{\xi}{\partial \xi}\left(\overline{u_2 c} - \frac{\nu_c}{X_2}\frac{\partial C}{\partial \xi}\right). \tag{7}$$

2.2. *The turbulence model*

The purpose of this section is to provide a closed set of equations for the correlations $\overline{u_1 u_3}$, $\overline{u_2 c}$ and $\overline{u_3 c}$. The approach to be adopted has become known as an 'algebraic stress model' [16]. It is basically a second-moment closure (i.e. one based on a closure of the exact transport equations for the Reynolds stresses and heat fluxes) in which, by approximating the transport of $\overline{u_i u_j}$ and $\overline{u_i c}$ in terms of the transport of the turbulence kinetic energy, k and the mean square variance of the concentration, $\overline{c^2}$, algebraic rather than differential equations emerge for the Reynolds stresses and scalar fluxes. The closure approximations we adopt have been previously reported and discussed in the literature, particularly in [9–11]. Here, therefore, we shall not comment extensively on the physical basis of the forms used.

We write the Reynolds stress transport equations in the symbolic form:

$$\frac{\mathrm{D}\overline{u_i u_j}}{\mathrm{D}t} = P_{ij} - \varepsilon_{ij} + \phi_{ij} + \mathscr{D}_{ij}, \tag{8}$$

where the terms on the right side of (8) denote interactions which are conventionally labelled production (P_{ij}), dissipation (ε_{ij}), pressure-scrambling (ϕ_{ij}) and diffusion ($\mathscr{D}_{ij}$). No approximation is needed for the production terms which are exactly expressible as

$$P_{ij} = -\left\{\overline{u_i u_k}\frac{\partial U_j}{\partial x_k} + \overline{u_j u_k}\frac{\partial U_i}{\partial x_k}\right\}.$$

At high Reynolds numbers dissipation occurs in the finest-scale motions that may usually be regarded as isotropic. The process ε_{ij} is thus expressible in terms of the dissipation rate of turbulence kinetic energy:

$$\varepsilon_{ij} = \tfrac{2}{3}\delta_{ij}\varepsilon.$$

Approximation of the pressure-scrambling processes is complicated by the fact that there are several contributions to the total that need to be separately

accounted for. We here adopt the scheme recently applied in [11] to explain the hitherto paradoxical response to stable stratification of the lower region of the atmospheric boundary layer. We write

$$\phi_{ij} = \phi_{ij1} + \phi_{ij2} + \phi_{ijw},$$

where

$$\phi_{ij1} = -C_1 \frac{\varepsilon}{k}\left(\overline{u_i u_j} - \frac{2}{3}\delta_{ij}k\right);$$

$$\phi_{ij2} = -C_2\left(P_{ij} - \frac{P_{kk}}{3}\delta_{ij}\right);$$

$$\phi_{ijw} = C_1' \frac{\varepsilon}{k}\left(\overline{u_k u_m}\, n_k n_m \delta_{ij} - \frac{2}{3}\overline{u_k u_i}\, n_k n_j - \frac{2}{3}\overline{u_k u_j}\, n_k n_i\right)\left(\frac{l}{x_n}\right) + C_2'\left(\phi_{km2}\, n_k n_m \delta_{ij} - \frac{2}{3}\phi_{ik2}\, n_k n_j - \frac{2}{3}\phi_{jk2}\, n_k n_i\right)\left(\frac{l}{x_n}\right).$$

Here the n terms denote unit vectors normal to the wall (i.e. the ground) l is the turbulence length scale, $k^{3/2}/\varepsilon$ and x_n is the normal distance from the point in question to the ground. In the outer region of a turbulent boundary layer the length scale is usually fairly uniform so the influence of ϕ_{ijw} diminishes with increasing distance from the ground (indeed, physically the term is accounting for the reflections of pressure pulses from the ground).

The diffusive transport term is handled indirectly. We take the term to the left side of equation (8) and following Rodi [17] write:

$$\left(\frac{\mathrm{D}\overline{u_i u_j}}{\mathrm{D}t} - \mathscr{D}_{ij}\right) = \frac{\overline{u_i u_j}}{k}\left(\frac{\mathrm{D}k}{\mathrm{D}t} - \mathscr{D}_k\right), \tag{9}$$

where $\mathscr{D}_k$ denotes the diffusive transport of turbulence energy. From the turbulence energy equation, however,

$$\left(\frac{\mathrm{D}k}{\mathrm{D}t} - \mathscr{D}_k\right) = \frac{1}{2}P_{kk} - \varepsilon \tag{10}$$

and we thus use the RHS of (10) instead of the LHS in (9).

With the above approximations, an algebraic set of equations emerge for $\overline{u_i u_j}$ which, for the plane two-dimensional thin shear flows considered here, lead to the following expressions for each of the components:

$$\overline{u_1^2} = \frac{2}{3}k\left[R_k\left(3 - 2C_2 + C_2C_2'\frac{l}{x_3}\right) + C_1 - 1 + C_1'\frac{\overline{u_3^2}}{k}\frac{l}{x_3}\right] \Big/ (C_1 + R_k - 1) \tag{11}$$

$$\overline{u_3^2} = \frac{2}{3}k\left[R_k\left(C_2 - 2C_2C_2'\frac{l}{x_3}\right) + C_1 - 1\right] \Big/ \left(C_1 + 2C_1'\frac{l}{x_3} + R_k - 1\right) \tag{12}$$

$$\overline{u_2^2} = \frac{2}{3}k\left[R_k\left(C_2 + C_2C_2'\frac{l}{x_3}\right) + C_1 - 1 + C_1'\frac{\overline{u_3^2}}{k}\frac{l}{x_3}\right] \Big/ (C_1 + R_k - 1) \tag{13}$$

$$\overline{u_1 u_3} = \frac{k}{\varepsilon}\overline{u_3^2}\frac{\partial U_1}{\partial x_3}\left(1 - C_2 + \frac{3}{2}C_2C_2'\frac{l}{x_3}\right) \Big/ \left(C_1 + R_k - 1 + \frac{3}{2}C_1'\frac{l}{x_3}\right). \tag{14}$$

where for brevity R_k stands for the ratio of the generation: dissipation rates of turbulence energy.

Equation (10), from which the turbulence energy is obtained, still contains the diffusive transport and dissipation rates as unknowns. We adopt the simple Daly–Harlow [18] model of the former process (where the term is to be thought of as accounting for transport due to both pressure and velocity fluctuations):

$$\mathscr{D}_k = \frac{\partial}{\partial x_l}\left(C_s\frac{k}{\varepsilon}\overline{u_j u_l}\frac{\partial k}{\partial x_j}\right). \tag{15}$$

The energy dissipation rate is obtained from its own transport equation:

$$\frac{\mathrm{D}\varepsilon}{\mathrm{D}t} = \frac{1}{2}c_{\varepsilon 1}P_{kk}\frac{\varepsilon}{k} - c_{\varepsilon 2}\frac{\varepsilon^2}{k} + \frac{\partial}{\partial x_j}\left(C_\varepsilon\frac{k}{\varepsilon}\overline{u_j u_l}\frac{\partial \varepsilon}{\partial x_l}\right). \tag{16}$$

For the two-dimensional, steady flow fields considered in the present study equations (10) and (16) take the following form:

$$U_1\frac{\partial k}{\partial x_1} + U_3\frac{\partial k}{\partial x_3} = -\overline{u_1 u_3}\frac{\partial U_1}{\partial x_3} - \varepsilon + \frac{\partial}{\partial x_3}\left(C_s\frac{k}{\varepsilon}\overline{u_3^2}\frac{\partial k}{\partial x_3}\right) \tag{17}$$

$$U_1\frac{\partial \varepsilon}{\partial x_1} + U_3\frac{\partial \varepsilon}{\partial x_3} = -c_{\varepsilon 1}\frac{\overline{u_1 u_3}}{k}\varepsilon\frac{\partial U_1}{\partial x_3} - C_{\varepsilon 2}\frac{\varepsilon^2}{k} + \frac{\partial}{\partial x_3}\left(C_\varepsilon\frac{\overline{ku_3^2}}{\varepsilon}\frac{\partial \varepsilon}{\partial x_3}\right). \tag{18}$$

Approximation of the turbulent scalar fluxes $\overline{u_i c}$ follows a parallel route to that of the Reynolds stresses. The transport equation for $\overline{u_i c}$ may be written:

$$\left(\frac{\mathrm{D}\overline{u_i c}}{\mathrm{D}t} - \mathscr{D}_{ic}\right) = -\overline{u_i u_j}\frac{\partial C}{\partial x_j} + P_{ic} + \phi_{ic} + \varepsilon_{ic}, \tag{19}$$

where the processes denoted by the symbols are production rate of $\overline{u_i c}$ by mean strain (P_{ic}), destruction by molecular action (ε_{ic}), pressure scrambling (ϕ_{ic}), and diffusive transport ($\mathscr{D}_{ic}$).

The first is exactly expressible as

$$P_{ic} = -\overline{u_k c}\frac{\partial U_i}{\partial x_k},$$

the second is zero in locally isotropic turbulence (and is henceforth neglected) while, following [11], the influential correlations between pressure and scalar gradient fluctuations are approximated as

$$\phi_{ic} = \phi_{ic1} + \phi_{ic2} + \phi_{icw}, \tag{20}$$

where

$$\phi_{ic1} = -C_{1c}\left(\frac{\varepsilon}{k}\right)\overline{u_i c}\,; \quad \phi_{ic2} = -C_{2c}P_{ic}$$

$$\phi_{icw} = +C'_{1c}\frac{\varepsilon}{k}\overline{u_k c}\,\underset{\sim}{n_i}\,\underset{\sim}{n_k}\,(l/x_n) + C'_{2c}\phi_{lc,z}\,\underset{\sim}{n_i}\,\underset{\sim}{n_k}\,(l/x_n)$$

and C_{1c}, C_{2c}, C'_{1c}, and C'_{2c} are constants.

As in the stress equations, the diffusive transport term is grouped with the convection term and following [19] these are then jointly expressed as

$$\left(\frac{\mathrm{D}\overline{u_i c}}{\mathrm{D}t} - \mathscr{D}_{u_i c}\right) = \frac{\overline{u_i c}}{2}\left[\frac{(P_c - \varepsilon_c)}{\overline{c^2}} + \frac{(\frac{1}{2}P_{ii} - \varepsilon)}{k}\right], \tag{21}$$

where P_c and ε_c are the production and dissipation rates of $\overline{c^2}$, the mean square variance of concentration fluctuations.

For the present we assume $P_c = \varepsilon_c$ which eliminates the first term on the right of equation (21). This practice is not consistent with that followed in formulating the Reynolds stresses. Consistency would, however, require solution of additional transport equations for $\overline{c^2}$ and ε_c which, in the present case, are three-dimensional quantities. The computational effort required for this is quite substantial, besides which, no extensively tested modelled equation for ε_c is yet available; for these reasons the simpler treatment is currently preferred. Insertion of equations (20) and (21) into equation (19) thus leads to the following equations for the scalar flux components:

$$\overline{u_1 c} = \frac{k}{\varepsilon}\left[-\overline{u_1 u_3}\frac{\partial C}{\partial x_3} + \overline{u_3 c}\frac{\partial U_1}{\partial x_3}(C_{2c} - 1)\right] \Big/ \left(\frac{R_k - 1}{2} + C_{1c}\right), \tag{22}$$

$$\overline{u_2 c} = -\frac{k}{\varepsilon}\overline{u_2^2}\frac{\partial C}{\partial x_2} \Big/ \left(\frac{R_k - 1}{2} + C_{1c}\right), \tag{23}$$

$$\overline{u_3 c} = -\frac{k}{\varepsilon}\overline{u_3^2}\frac{\partial C}{\partial x_3} \Big/ \left(\frac{R_k - 1}{2} + C_{1c} + C'_{1c}C_{1c}\frac{l}{x_3}\right). \tag{24}$$

The empirical coefficients appearing in equations (11)–(14), (17), (18), (22)–(24) take the magnitudes shown in Table 1. The values chosen are those recommended in [9] and [11].

Before proceeding to the method of solution, equations (17) and (18) are first presented in the x–η–η_h coordinate system:

$$\frac{\partial U_1 k}{\partial x} - \frac{1}{X_3}\eta_h\frac{\partial U_1 k}{\partial \eta_h}\frac{\mathrm{d}X_3}{\mathrm{d}x} + \frac{1}{X_3}\frac{\partial U_3 k}{\partial \eta_h} = -\frac{\overline{u_1 u_3}}{X_3}\frac{\partial U_1}{\partial \eta_h} - \varepsilon + \frac{1}{X_3}\frac{\partial}{\partial \eta_h}\left(C_s\frac{k}{\varepsilon}\frac{\overline{u_3^2}}{X_3}\frac{\partial k}{\partial \eta_h}\right) \tag{25}$$

$$\frac{\partial U_1 \varepsilon}{\partial x} - \frac{\eta_h}{X_3}\frac{\partial U_1 \varepsilon}{\partial \eta_h}\frac{\mathrm{d}X_3}{\mathrm{d}x} + \frac{1}{X_3}\frac{\partial U_3 \varepsilon}{\partial \eta_h} = -\frac{C_{\varepsilon 1}}{X_3}\frac{\varepsilon}{k}\overline{u_1 u_3}\frac{\partial U_1}{\partial \eta_h} - C_{\varepsilon 2}\frac{\varepsilon^2}{k} + \frac{1}{X_3}\frac{\partial}{\partial \eta_h}\left(C_\varepsilon\frac{k}{\varepsilon}\frac{\overline{u_3^2}}{X_3}\frac{\partial \varepsilon}{\partial \eta_h}\right). \tag{26}$$

Finally, equations (6), (25), (26) can all be cast into the generalized form

$$\frac{\partial U_1 \phi}{\partial x} - \frac{\eta}{x_3}\frac{\partial U_1 \phi}{\partial \eta_h}\frac{\mathrm{d}X_3}{\mathrm{d}x} + \frac{1}{X_3}\frac{\partial U_3 \phi}{\partial \eta_h} = S_\phi + \frac{1}{(X)_3^2}\frac{\partial}{\partial \eta_h}\left(\Gamma_\phi\frac{\partial \phi}{\partial \eta_h}\right), \tag{27}$$

where ϕ can be any of the variables U_1, k or ε and S and Γ_ϕ are given in Table 2 for the different variables.

3. METHOD OF SOLUTION

3.1. *Finite difference grid*

In the dispersal problems of interest the vertical dimension of the plume will typically be one or two orders of magnitude less than the thickness of the atmospheric boundary layer. Thus, a grid distribution that resolved the flow field economically would be too coarse for the concentration field; correspondingly, a grid fine enough to give numerically accurate results of the concentration would be uneconomical if used for the whole boundary layer. For these reasons independent grids are employed for the two fields; where required hydrodynamic information is transferred by interpolation from the flow grid to the scalar one. When, however, a concentration grid node lies below the hydrodynamic grid node nearest to the ground, the well-known semi-logarithmic 'law of the wall' for velocity provides the interpolation formula.

Figures 1 and 2 show sections in the x_1–x_3 and x_1–x_2 planes of the grids employed. The quantities X_3, X_3^U and X_3^l, appearing in Fig. 1 mean:

- X_3: vertical distance from ground to upper boundary of hydrodynamic grid;
- X_3^U: vertical distance from ground to upper boundary of concentration grid;
- X_3^l: vertical distance from ground to lower edge of concentration grid.

Table 1. Constants employed in turbulence model

Constant	C_1	C_2	C'_1	C'_2	$C_{\varepsilon 1}$	$C_{\varepsilon 2}$	C_ε	C_s	C'_{1c}	C'_{2c}	C'_{1c}	C'_{2c}
Value	1.80	0.60	0.52	0.28	1.44	1.90	0.15	0.25	0.30	0.33	0.50	0

Table 2. S_ϕ and Γ_ϕ for $\phi = U$, k and ε

ϕ	Γ_ϕ	S_ϕ
U	$-X_3\overline{u_1u_3}/(\partial U_1/\partial\eta_h)$	$-\frac{1}{\rho}\frac{dP}{dx}$
k	$C_S\frac{k}{\varepsilon}\overline{u_3^2}$	$-\frac{\overline{u_1u_3}}{X_3}\frac{\partial U_1}{\partial\eta_h}-\varepsilon$
ε	$c_\varepsilon\frac{k}{\varepsilon}\overline{u_3^2}$	$-C_{\varepsilon1}\frac{\varepsilon}{k}\frac{\overline{u_1u_3}}{X_3}\frac{\partial U_1}{\partial\eta_h}-C_{\varepsilon2}\frac{\varepsilon^2}{k}$

The quantity X_2 appearing in Fig. 2 is the lateral distance from the plane of symmetry to the edge of the (concentration) grid. Also shown on Figs. 1 and 2 are samples of the 'control volumes' employed in the derivation of the finite-difference equations; the boundaries of these volumes lie midway between adjacent nodes except at the boundaries of the integration domain where the edges of the control volume and the nodes coincide. The scalar quantities k and ε are located at the nodes of the concentration grid. On each grid the velocities are displaced relative to nodes so that they lie midway along, and normal to, the sides of the control volumes as indicated in Fig. 1 (the vertical and horizontal arrows indicate the locations of the cross-stream and streamwise velocities respectively).

3.2. *The finite difference equations*

Integration of equation (7) over a control volume such as shown in Fig. 1, coupled with the assumption of a linear variation of C between grid points in the vertical and lateral directions and a stepwise variation in the streamwise direction leads to

$$a^P_{i,j}C_{i,j,k} = a^N_{i,j}C_{i,j+1,k} + a^S_{i,j}C_{i,j-1,k} + a^E_{i,j}C_{i+1,j,k} + a^W_{i,j}C_{i-1,j,k} + a^U_{i,j}C_{i,j,k-1}, \quad (28)$$

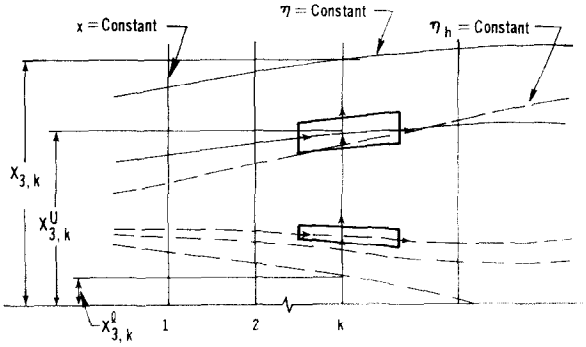

FIG. 1. Velocity and concentration grids in x_1–x_3 plane.

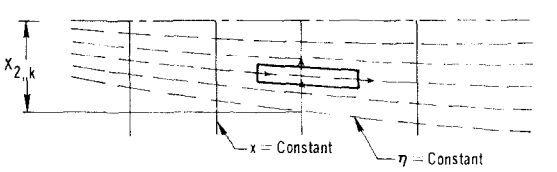

FIG. 2. Concentration grid in x_1–x_2 plane.

where the subscripts i, j and k identify the grid-node locations in the lateral, and streamwise directions respectively, $a^N_{i,j}, a^S_{i,j}\ldots$ etc. express the combined effect of convection and diffusion and

$$a^P_{i,j} = \sum_{\theta = N,S,\ldots} a^\theta_{i,j}.$$

Similarly, integration of equation (27) over the control volume (on the hydrodynamic grid) shown in Fig. 1 gives the following finite difference equation for the variable ϕ:

$$a^P_j\phi_{j,k} = a^N_j\phi_{j+1,k} + a^S_j\phi_{j-1,k} + a^U_j\phi_{j,k-1} + S^P_j\phi_{j,k} + S^U_j. \quad (29)$$

The subscripts j and k again locate the grid in the vertical and longitudinal directions; $a^N_j, a^S_j, \ldots$ etc. are (one-dimensional) coefficients expressing the effects of both convection and diffusion while

$$a^P_j \equiv \sum_{\theta = N,S,\ldots} a^\theta_j$$

and

$$S^P_j\phi_{j,k} + S^U_j \equiv \int_x^{x+\Delta x}\int_{\eta_h}^{\eta_h+\Delta\eta_h} S_\phi X_3\,dx\,d\eta_h.$$

3.3. *Solution of the finite-difference equations*

Solution of equations (28) and (29) proceeds in a stepwise manner, starting from the upstream end of the integration domain and proceeding step-by-step downstream. Thus in equation (28) and (29) the values of S^U_j, S^P_j, C_{k-1} and ϕ_{k-1} are known from the previous step; only values having k subscripts are unknown. To solve equation (28), the values of C with subscripts $i-1$ and $i+1$ (i.e. neighbours to node i in the lateral direction), are temporarily assumed known. A Gaussian elimination method is then applied to solve for the concentrations along the vertical grid line j. Thereafter solution proceeds to the next vertical grid line, $j+1$, and so on until all the concentration values lying in the cross-stream plane have been obtained. This sequence of operations completes a 'sweep'. Because the levels of C are in fact dependent on the levels in the adjacent columns, more than one sweep is required to obtain a satisfactory solution. The satisfactoriness of the solution is assessed by calculating the residual source R which is defined as

$$R = \sum_{\text{all nodes}} \left| a^N_{i,j}C_{i,j+1,k} + a^S_{i,j}C_{i,j-1,k} + a^E_{i,j}C_{i+1,j+k} + a^W_{i,j}C_{i-1,j,k} + a^U_{i,j}C_{i,j,k-1} - a^P_{i,j}C_{i,j,k}\right|.$$

The lower the value of R, the smaller the numerical error in the solution. In the case of the 2-dimensional variables (i.e. U_1, k, or ε) the absence of lateral neighbouring columns renders one application of the Gauss-elimination method 'exact'.

3.4. *Boundary and initial conditions*

The upstream conditions employed are normally

those given by experiment, if such data exist. When these are not available a step function is assumed for the concentration profile, i.e. the value of the concentration is assumed zero everywhere except at the location of the source.

The following boundary conditions are applied as the calculations proceed downstream. At upper and lower boundaries of the plume the concentration is set to zero provided the lower boundary is above the ground level; at a plane of symmetry or when the lower edge of the plume reaches the ground the mass flux of pollutant normal to this boundary is assumed to be zero. For the flow field, the value of k, ε and U_1 are given their free-stream values at the outer boundary while, at the wall, the no-slip condition for U_1 is applied. Due to highly non-linear variation of the velocity near the wall a match is made to the logarithmic law of the wall outside the viscosity affected region. The turbulence quantities k and l are prescribed at the nodes adjacent to the wall; the energy dissipation rate there is equated to the generation rate of k (by assuming local equilibrium) while the turbulent kinetic energy is taken as four times the kinematic wall shear stress as indicated by Klebanoff's data [20].

4. RESULTS AND DISCUSSION

To assess the performance of the expanding grid and the numerical procedure, comparison was first made between the predicted and analytical solutions for diffusion from a point release in a homogeneous flow field. The numerical results were found to be indistinguishable from the analytical solution quoted by Hinze [21]. A test of the algebraic stress model was accomplished by simulating Klebanoff's [20] experiment of a two-dimensional turbulent flow over a smooth flat plate. Predictions are compared with experimental values of the mean velocity and shear stress $\overline{u_1 u_3}$ in Fig. 3, the level of agreement is considered to be satisfactory. Comparisons for the normal stresses are shown in Fig. 4. The predicted stress levels in the outer region of the boundary layer are found to be slightly higher than the experimental values though this may be due in part to different definitions of δ between experiment and computation (reference [20] does not provide a precise definition).

The principal plume-dispersal calculations focused on four cases:

(i) a ground level release from a line source,
(ii) an elevated line source,
(iii) a ground release from a point source and
(iv) an elevated release from a point source.

In all cases the releases occurred within a turbulent, nominally two-dimensional boundary layer flowing over a plane, hydrodynamically smooth surface. Grid-independent solutions were obtained with 20 cross-stream nodes for the hydrodynamic field and a 15×15 grid for the concentration.*

Figure 5 shows the enlargement of the half height λ_3

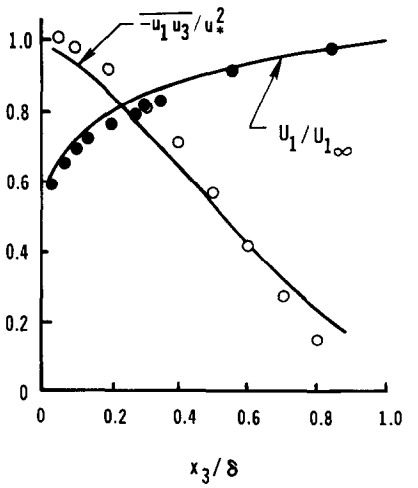

FIG. 3. Velocity and shear stress across flat plate boundary layer: —— predictions; ○, ● experiments, Klebanoff [20].

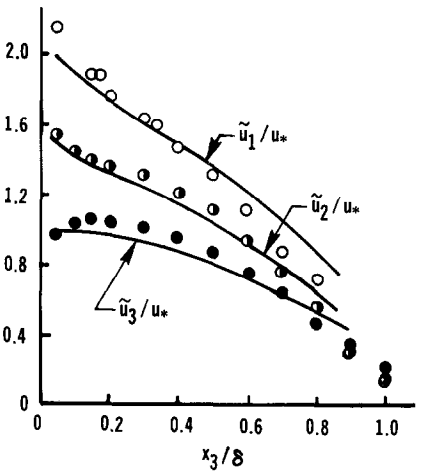

FIG. 4. Turbulence intensity profiles across flat plate boundary layer: —— predictions; ○, ◑, ● experiments, Klebanoff [20].

with distance downstream of a plume emitted from a ground level line source.† The results show good agreement with Poreh and Cermak's [22] experimental data. These authors report that for an 'intermediate zone' extending to distances up to 18δ from the point of release λ_3 is well fitted by the formula:

$$\lambda_3 = 0.076\, x^{0.8}, \tag{30}$$

implying that λ_3 is independent of both the boundary layer thickness and the free stream velocity. This behaviour is confirmed by the present study. In Fig. 6, for example, predictions of λ_3 for two values of boundary layer thickness are in good agreement with

*For two-dimensional plumes only 3 grid lines were employed in the lateral direction.

†The half height is defined as the height at which any streamwise position the concentration level has fallen to half its maximum.

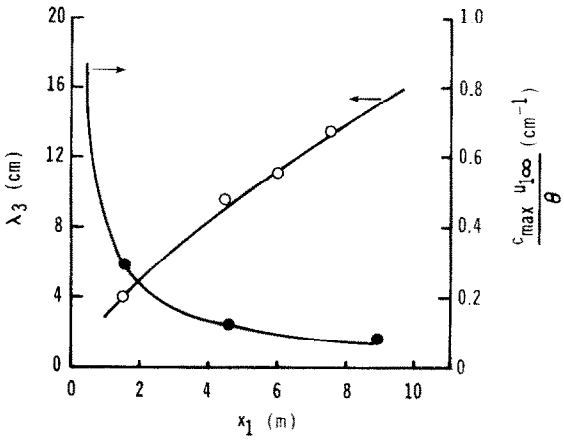

FIG. 5. Variation of width and maximum concentration from a ground-level, line source: —— prediction; ○, ● measurement, Poreh and Cermak [22].

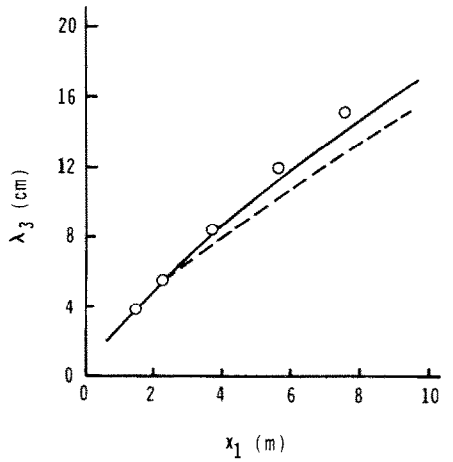

FIG. 6. Effect of free stream velocity on width of line source: ○ fit given by [22]; predictions: —— $U_{1\infty}$ = 2.74, - - - $U_{1\infty}$ = 7.99.

equation (30) for values of x less than 18δ; further downstream, however, the dispersal pattern becomes sensitive to boundary-layer thickness. Figure 7 shows the effect of varying the mainstream velocity on the dispersal. Again, for values of x/δ less than 18, λ_3 is independent of the velocity while at greater distances a slightly lower dispersal rate is observed for the higher velocity. The variation of maximum concentration with downstream distance is shown in Fig. 6. Here again the predictions show close agreement with the experimental data of Poreh and Cermak. Figure 8 indicates that the profiles of concentration across the boundary layer are approximately self-similar in the 'intermediate region'; again the calculated profiles display a behaviour that agrees well with the experimental fit for this region. It should be added that exact similarity is not to be expected, for it can be shown (El Tahry [23]) that when the concentration equation is suitably non-dimensionalized a weak dependence on x appears, mainly because of the dependence of (λ_3/δ) on x.

The predictions of an elevated line source simulated the experiments of Paranthoen and Trinité [24], in which an electrically heated wire was placed parallel to the wall and perpendicular to the mainstream velocity. The Reynolds number of the flow, based on boundary layer thickness and mainstream velocity was 17 100; the ratio of height of release to boundary layer thickness was 0.5. Calculations of the vertical temperature distribution are presented at several downstream locations in Fig. 9. Initially the predicted plume seems to have diffused slightly faster than the experimental one. This discrepancy is we believe due to the use of time and length scales characteristic of the *velocity* rather than the scalar turbulent fluctuations; further discussion is provided in reference [15] and in Section 5. Further downstream the experimental data fall below the predicted results, which may be attributed to a loss of heat through the wall influencing the experi-

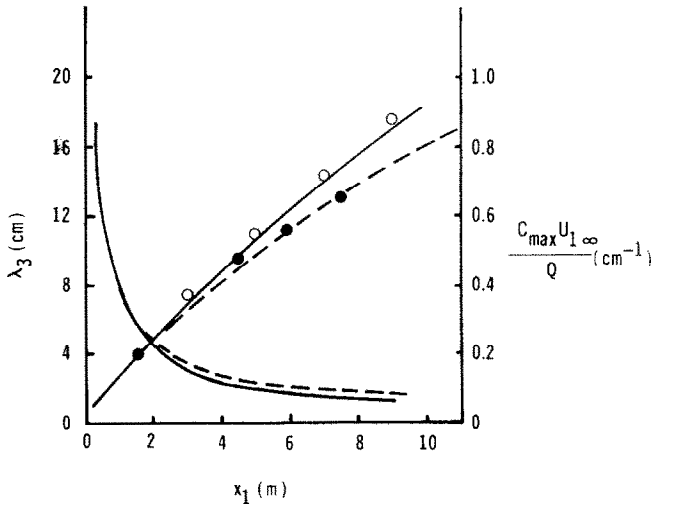

FIG. 7. Effect of initial thickness of boundary layer on development of line source: ○ proposed algebraic fit to experiments [22], ● experimental data [22]; predictions, $U_{1\infty}$ = 4.87 m/s: - - - δ_0 = 0.127 m, δ_0 = 0.28 m.

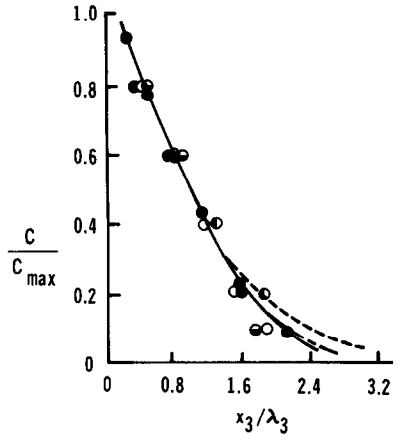

FIG. 8. Normalized concentration profiles at different downstream stations: ● fit to experiments [22]; predictions of Wassel and Catton: ◒ — $x_1 = 2.13$ m; ○ — $x_1 = 3.66$ m; ◐ — $x_1 = 5.18$ m; present predictions: – – – $x_1/\delta = 3.2$; — · — $x_1/\delta = 10$; —— $x_1/\delta = 13$ and 18.

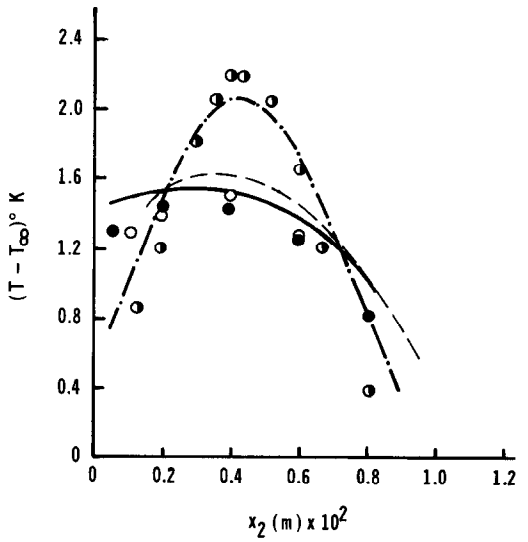

FIG. 9. Temperature profiles across air elevated line source: experiments [24] ◑ — $x_1 = 0.075$ m; ○ — $x_1 = 0.135$ m; ● — $x_1 = 0.165$ m; predictions: — · — $x_1 = 0.075$; – – – $x_1 = 0.135$; —— $x_1 = 0.165$.

mental data (the experimental temperature profiles suggest a non-zero slope at the wall). Despite these discrepancies the overall agreement is considered to be reasonably good.

The case of the ground release from a point source is considered in Figs. 10–12. Figure 10 shows the variation of the vertical and lateral half widths λ_3 and λ_2 with downstream distance together with the experimental data of Malhotra and Cermak [25] and Solal [26]. The predictions agree well with both sets of experiments of the vertical spread while, for the lateral dispersal, close agreement with Malhotra and

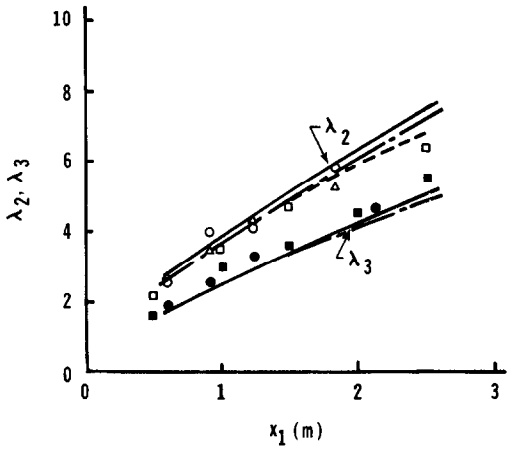

FIG. 10. Growth of half-widths of ground level point source: ○, ● $U_{1\infty} = 2.74$ m/s [25]; △ $U_{1\infty} = 4.57$ m/s [25]; □, ■ [26]; — · —, – – –, —— present predictions.

Cermak's data is observed. Discrepancies of up to 14% are noted for Solal's data, however, a disparity that may be due to convergence of the boundary-layer streamlines.

The distribution of the maximum concentration in the plume with downstream distance is shown in Fig. 11. The calculations are found to agree well with both sets of experimental data. Predictions of the lateral profiles of the relative concentration C/C_{max} are shown in Fig. 12 for different heights. These profiles display similarity at different x locations over the region considered. The results are in complete agreement with Malhotra and Cermak's empirical fit:

$$\frac{C}{C_{max}} = \exp 0.693\left\{-\left(\frac{x_2}{\lambda_2}\right)^2 - \left(\frac{x_3}{\lambda_3}\right)^{1.4}\right\}.$$

Dispersal from an elevated point source is considered in Figs. 13–14. Here the source is placed at a height 0.645δ. The Reynolds number based on the mainstream velocity and boundary layer thickness was approximately 9330 which corresponds to an experiment reported by Davar [3]. In Fig. 13 the quantities β_3, β_2 are plotted as a function distance x^*; also shown is the variation of β (the height of maximum concentration) with x. In general the calculations are in reasonable agreement with Davar's data, except that they underestimate the lower value of β_3.† While no certain explanation can be given for the discrepancy, it might be said that uncertainties existed in the upstream experimental velocity profiles due to the artificial thickening. Finally, Fig. 14 compares Davar's measurements of lateral concentration profiles with the computed behavior at different heights at a particular x; agreement is reasonably good.

* β_3 is the value of x_3 in the plane of symmetry where $C = 0.75C_{max}$ and β_2 is the value of x_2 where $C = 0.75C_{max}$ at the height of C_{max}.

† β_3 has two values at each value of x corresponding to positions in the upper and lower parts of the plume.

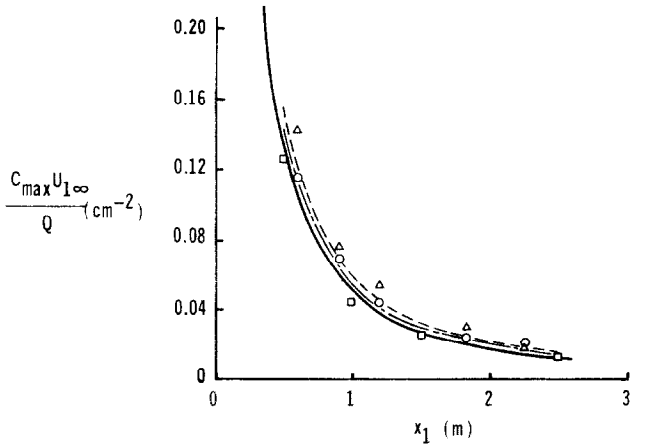

FIG. 11. Decay of maximum concentration in a ground level point source (for key see Fig. 10).

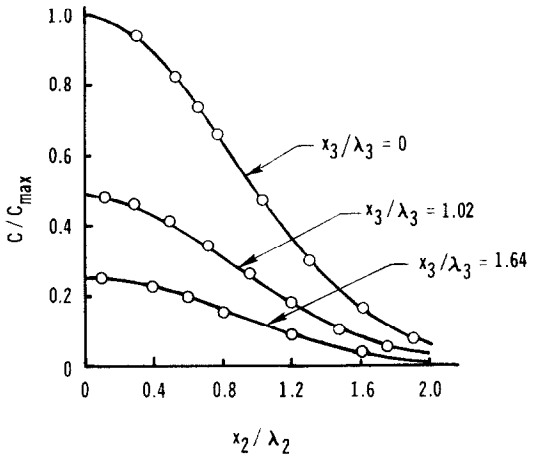

FIG. 12. Lateral concentration profiles for ground level point source: ○ $C/C_{max} = \exp -0.693\ [(x_2/\lambda_2)^2 + (x_3/\lambda_3)^{1.4}]$, [25]; —— present predictions.

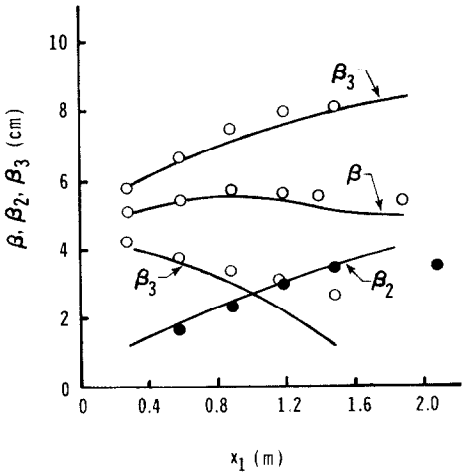

FIG. 13. Spreading characteristics of an elevated point source: ○, ● experiments, Davar [3]; —— present predictions.

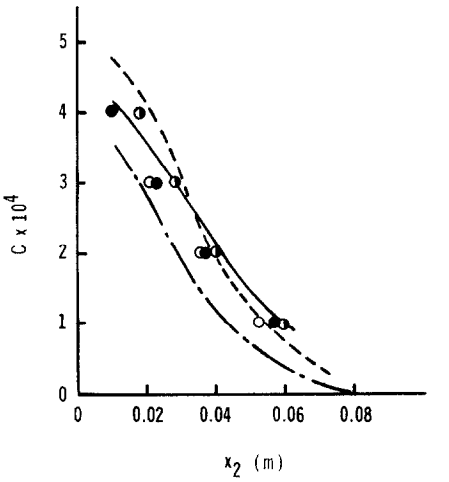

FIG. 14. Concentration profiles in elevated point source at $x_1 = 0.914$.

x_3	Experiment [3]	Present predictions
0.0385	●	——
0.0554	○	- - -
0.072	○	- · -

5. CONCLUDING REMARKS

The computational scheme presented in the paper has been shown to give a generally satisfactory account of plume dispersal in the four test cases considered. Although based upon a fairly elaborate physical and numerical treatment, the scheme is sufficiently economical for use as the basis for extensive safety surveys. The economy arises from the use of independent finite-difference grids for the scalar and flow-field variables and from the use of the algebraic-stress-modelling hypothesis to reduce the transport equations for the Reynolds stress and scalar fluxes to a set of explicit algebraic relations.

Although the present study has limited attention to neutrally buoyant tests the turbulence model adopted [11] was developed specifically to provide an explanation of the behavior of the atmospheric boundary layer under highly stratified conditions. It may thus be reasonably expected that the present scheme would provide useful dispersal predictions under realistic atmospheric conditions, at least so far as effects of stratification are concerned.

In one respect however the present model does need improvement. The scheme contains only one characteristic turbulent length scale, $k^{3/2}/\varepsilon$ for both the velocity and the scalar fields. In the atmospheric boundary layer, however, especially near the point of release, far smaller scales characterize the dispersal of the pollutant than are typical of the flow field. As Lewellyn and Teske [15] have noted, no serious errors are introduced by the present practice for a ground-level release because, near the ground, velocity scales are appropriately small: the problem only becomes serious as the height of the release is increased. While, in the laboratory studies considered here, the errors introduced appear to be fairly small (c.f. Fig. 11), the effect in the atmospheric boundary layer could well be substantial because the ratio of plume width: boundary-layer height is typically some two orders of magnitude smaller than in the cases here examined.

Acknowledgements — The research reported herein has been supported by the Safety and Reliability Directorate of the United Kingdom Atomic Energy Authority. We are pleased to acknowledge the help and encouragement provided by Dr. A. J. H. Goddard who jointly directs the project. Our thanks are due also to Ms. L. S. Majesky who has prepared the manuscript for publication. Author's names appear alphabetically.

REFERENCES

1. F. Pasquill, *Atmospheric Diffusion.* Van Nostrand, Amsterdam (1962).
2. H. D. Slade, *Meteorology and Atomic Energy*, U.S. Atomic Energy Commission, Office of Information (1968).
3. K. S. Davar, Ph.D. thesis, Colorado State University, Fort Collins, Colorado (1961).
4. F. B. Smith, *J. Fluid Mech.* **2**, 49 (1957).
5. C. S. Yih, Similarity solution of a specialised diffusion equation, *Trans. Am. geophys. Un.* **33**, 356 (1951).
6. W. K. Ragland and J. G. Dennis, *Int. J. Heat Mass Transfer* **7**, 1083 (1964).
7. A. T. Wassel and I. Catton, *Int. J. Heat Mass Transfer* **20**, 383–391 (1977).
8. S. V. Patankar and D. B. Spalding, *Heat and Mass Transfer in Boundary Layers.* International Textbook (1970).
9. B. E. Launder, G. J. Reece and W. Rodi, *J. Fluid Mech.* **68**, 537–566 (1975).
10. B. E. Launder, Heat and mass transport, in *Topics in Applied Physics* (Edited by P. Bradshaw), Volume 12, Chapter 6. Springer (1976).
11. M. M. Gibson and B. E. Launder, Ground effects on pressure fluctuations in the atmospheric boundary layer, *J. Fluid Mech.* **86**, 491–511 (1978).
12. J. C. Wyngaard and O. R. Coté, The evolution of a convective planetary boundary layer — A higher order closure model study, *Boundary-Layer Meteorol.* **7**, 289 (1974).
13. J. L. Lumley and B. Khajeh-Nouri, Computational modelling of turbulent transport, *Adv. Geophys.* **18A**, 169 (1974).
14. C. du P. Donaldson, R. D. Sullivan and H. Rosenbaum, A theoretical study of the generation of atmospheric-clear air turbulence, *AIAA Jl* **10**(2), 162 (1972).
15. W. J. Lewellyn and M. E. Teske, *Boundary-Layer Meteorol.* **10**, 69 (1976).
16. B. E. Launder, An improved algebraic stress model of turbulence, Imperial College Mechanical Engineering Department Report TM/TN/A/9 (1971).
17. W. Rodi, The prediction of free turbulent boundary layers by use of a two-equation model of turbulence, Ph.D. thesis, Imperial College, London University (1974).
18. B. J. Daly and F. M. Harlow *Physics Fluids* **13**, 2634–2649 (1970).
19. M. M. Gibson and B. E. Launder, On the calculation of horizontal, turbulent free shear flows under gravitational influence, *Trans. ASME, Ser. C. J. Heat Transfer* **98C**, 81–87 (1976).
20. P. S. Klebanoff, National Advisory Committee Aeronautical Technical Notes 3133 (1954).
21. J. Hinze, *Turbulence.* McGraw-Hill, New York (1975).
22. M. Poreh and J. G. Cermak, *Int. J. Heat Mass Transfer* **7**, 1083 (1964).
23. S. El Tahry, Ph.D. thesis, University of London (1979).
24. P. Paranthoen and M. Trinité, *C. r. hebd. Séanc. Acad. Sci., Paris* **276**, Série A, 1473 (1973).
25. R. C. Malhotra and J. E. Cermak, *Int. J. Heat Mass Transfer* **7**, 169 (1964).
26. J. Solal, Etude experimentale de la diffusion de masse dans une couche limite turbulente en ecoulement neutre et en ecoulement stratifié instable, Thèse Docteur-Ingénieur, Université Claude Bernard de Lyon, France (1972).

DISPERSION BI ET TRIDIMENSIONNELLE D'UN SCALAIRE PASSIF DANS UNE COUCHE LIMITE TURBULENTE

Résumé — Un modèle numérique est décrit pour prédire le transport d'un contaminant scalaire passif à travers la couche limite. Le modèle inclut une fermeture, pour les contraintes turbulentes et pour les flux thermiques, basée sur le modèle des références [9–11]. Le traitement numérique utilise différentes grilles aux différences finies pour les champs de vitesse et de scalaire chacun d'eux pouvant être traité indépendamment dans la direction de l'écoulement de façon à atteindre les régions où existent des gradients sensibles des variables. Des calculs sont traités pour des sources linéaires ou ponctuelles avec des débits faibles ou élevés. Les calculs sont généralement en accord encourageant avec les mesures.

DIE ZWEI- UND DREIDIMENSIONALE VERTEILUNG EINES PASSIVEN SKALARES IN EINER TURBULENTEN GRENZSCHICHT

Zussamenfassung—Zur Vorhersage des Transports einer passiven skalaren Verunreinigung durch eine turbulente Grenzschicht wird ein numerisches Berechnungsverfahren beschrieben. Das Verfahren enthält einen algebraischen Ansatz für die Berücksichtigung der turbulenten Schubspannungen und Wärmeströme nach dem Verfahren der Literaturangaben [9–11]. Ein Hauptgesichtspunkt der zahlenmäßigen Behandlung ist die Verwendung verschiedener Netze endlicher Differenzen für die Geschwindigkeits- und Skalarfelder, welche unabhängig so weit in die Abwindrichtung ausgedehnt werden können, daß sie gerade die Gebiete überdecken, wo bedeutende Gradienten der maßgeblichen Veränderlichen bestehen. Von Berechnungen für die Ausbreitung von Linien- und Punktquellen mit Auslässen sowohl am Boden als auch in erhöhter Position wird berichtet. Die Berechnungen sind allgemein in ermutigender Übereinstimmung mit dem gemessenen Verhalten.

ДВУХ- И ТРЕХМЕРНОЕ РАСПРЕДЕЛЕНИЕ ПАССИВНОГО СКАЛЯРА В ТУРБУЛЕНТНОМ ПОГРАНИЧНОМ СЛОЕ

Аннотация — Описана схема для численного расчета переноса пассивной скалярной примеси в турбулентном пограничном слое. Схема включает алгебраическое замыкание турбулентных напряжений и тепловых потоков, основанное на модели, изложенной в [9–11]. Отличительной особенностью предлагаемой схемы является использование различных конечно-разностных сеток для полей скорости и скаляра, каждую из которых можно независимо от другой продлить в направлении течения, так чтобы включить области с существенными градиентами соответствующих зависимых переменных. Приведены расчеты для диффузии линейных и точечных источников, расположенных на различных уровнях в слое. Результаты расчетов удовлетворительно согласуются с измеренными значениями.